Wrapping Carbon Nanotubes in Pyrene-Containing Poly(phenylacetylene) Chains: Solubility, Stability, Light Emission, and Surface Photovoltaic Properties

Wang Zhang Yuan,[†] Jing Zhi Sun,[†] Yongqiang Dong,[†,‡] Matthias Häussler,[‡] Feng Yang,[†] Hai Peng Xu,[†] Anjun Qin,[‡] Jacky W. Y. Lam,[‡] Qiang Zheng,[†] and Ben Zhong Tang*[,†,‡]

Department of Polymer Science & Engineering, Key Laboratory of Macromolecular Synthesis and Functionalization,[§] Zhejiang University, Hangzhou 310027, China, and Department of Chemistry, The Hong Kong University of Science & Technology, Clear Water Bay, Kowloon, Hong Kong, China

Received August 13, 2006; Revised Manuscript Received September 15, 2006

ABSTRACT: A group of pyrene-containing poly(phenylacetylene)s (PPAs) with high molecular weight (M_w up to ~170 000) were synthesized in high yields (up to ~96%). Simply mixing the polymers and multiwalled carbon nanotubes (MWNTs) in an appropriate solvent afforded the polymer/MWNT hybrids with MWNT contents up to ~25 wt %, which are soluble in common organic solvents such as chloroform and THF. The solubility can be as high as 637.5 mg/L in THF, thanks to the "additive effect" of the PPA skeleton and the pyrene pendants in solubilizing the MWNTs. The solubilization is realized through the spontaneous wrapping of the polymer chains round the MWNT shells, which is driving by the favorable $\pi-\pi$ interactions of the PPA skeleton and the pyrene rings with the MWNT walls. The P**2**(*5*)/MWNT hybrid is thermally stable, losing little of its weight when heated to 338 °C. The P**2**(*m*)/MWNT hybrids are electronically more conjugated and emit blue-green light more efficiently than their parent polymers upon photoexcitation. The surface photovoltaic cell fabricated from the P**2**(*5*)/MWNT hybrid is bipolar, suggesting an efficient photoinduced charge transfer between the two components, i.e., P**2**(*5*) and MWNT.

Introduction

Carbon nanotubes (CNTs) are of great interest in scientific research and technological innovation due to their unique nanostructures and novel materials properties.[1,2] Particularly, their remarkable electronic and optical properties[1−7] make them promising for such applications as nanosensors,[8] nanoelectrodes,[9] quantum wires,[10] molecular diodes,[11] and photoelectrochemical devices.[12−18] Several issues, however, must be addressed before the CNTs can be integrated into functional hybrids for fabrication of advanced devices. One of the most outstanding problems is their notorious intractability: CNTs are insoluble in any solvents and infusible at any temperatures before decomposing.

Two approaches, i.e., covalent[2,19,20] and noncovalent[21−23] functionalizations, have been used to improve the macroscopic processability of CNTs. Although the covalent functionalization of CNTs yields soluble samples and make some potential applications of CNTs feasible, the permanent structural changes caused by the chemical reactions unavoidably perturb their electronic conjugations. The change in the orbital hybridization from sp^2 to sp^3, for example, may result in undesirable deteriorations in their optical, electrical, and mechanical properties.

The noncovalent approach can confer new properties on the CNTs without destroying the electronic conjugation of their curled graphene sheets. Among all the routes for the noncovalent functionalization, wrapping CNTs in conjugated polymer chains is a particularly attractive one.[20k,21,24] It is well-known that conjugated polymers with macroscopic solubility and electrical semiconductivity have the potential to find high-tech applications in photoelectronic devices such as light-emitting diodes, photovoltaic cells, and field-effect transistors.[25] Wrapping CNTs in such polymer chains is expected to endow them with macroscopic processability and new photoelectronic properties.[20−23] On the other hand, CNTs may help enhance charge transport, electrical conduction, optical nonlinearity, mechanical strength, and chemical stability of the conjugated polymers.[20−23]

Polyacetylene is a prototypical conjugated polymer. Our group has synthesized a variety of substituted polyacetylenes, especially the derivatives of poly(phenylacetylene) (PPA).[26,27] The polymers have been found to exhibit an array of unique functional properties such as optical nonlinearity, liquid crystallinity, light emission, photoconductivity, and bioactivity.[26,27] We have been interested in the hybridization of soluble polyacetylenes with CNTs in the hope of generating macroscopically processable functional materials with combined advantageous attributes of the two components. In our previous study, we worked on wrapping CNTs with PPA chains and investigated the solution behaviors of the resultant hybrids as well as their optical properties.[21] Through the in-situ polymerization of phenylacetylene (PA) initiated by the transition-metal catalysts in the presence of multiwalled carbon nanotubes (MWNTs), soluble hybrids of PPA and MWNTs were produced, and the solutions of the hybrids were found to exhibit an impressively large optical limiting effect.[21]

In this work, we prepared several new homo- and copolymers of PAs bearing pyrene pendants, i.e., P**1**, P(**1**-*co*-PA) and P**2**(*m*) (Schemes 1 and 2). As mentioned above, we have previously demonstrated that wrapping by PPA chains has made MWNTs readily soluble in common organic solvents.[21] There have been several reports showing that pyrene derivatives can be noncovalently bound to CNTs, which has helped improve the

* Corresponding author: Ph +852-2358-7375; Fax +852-2358-1594; e-mail tangbenz@ust.hk.
[†] Zhejiang University.
[‡] The Hong Kong University of Science & Technology.
[§] Administrated by the Ministry of Education of the People's Republic of China.

10.1021/ma061856c CCC: $33.50
Published on Web 10/24/2006

Scheme 1

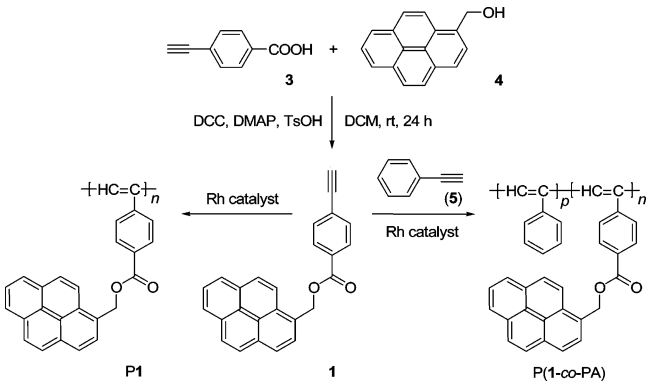

Scheme 2

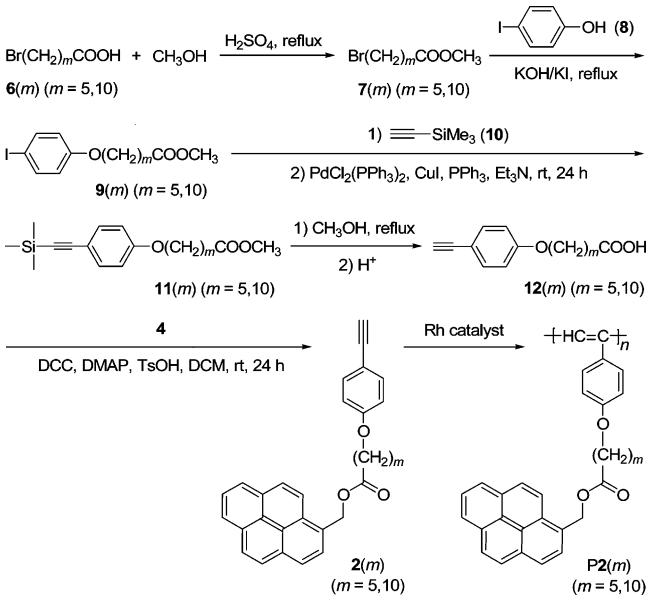

solubility of the CNTs in common organic solvents.[3,22,23e,28] It is envisioned that the PPA skeleton and the pyrene pendant may work synergistically and the "additive effect" may greatly enhance the solvating power of the pyrene-containing PPAs. Pyrene chromophore has been widely used as a fluorescent sensor for detecting structural changes as well as probing electronic processes in the chemical and biological systems.[29,30] The incorporation of the pyrene unit may provide a tool for sensing photoelectronic interactions in the PPA/CNT hybrids. Furthermore, the sterically bulky and thermally stable pyrene pendants are expected to serve as a "jacket",[26,27,31] which shields the polyene backbone from the attack by the thermolytic species, thus helping enhance the thermal stability of the polymers. In this paper, we report the design and synthesis of pyrene-containing PPAs and prove that the polymers are indeed excellent solvating agents for MWNTs. The PPA/MWNT hybrids show high thermal stability, bright photoluminescence, and efficient photoinduced charge transfer.

Experimental Section

Materials. THF was distilled under normal pressure from sodium benzophenone ketyl under argon immediately prior to use. Dichloromethane (DCM) was distilled under normal pressure over calcium hydride under argon before use. Triethylamine (TEA) was distilled and dried over potassium hydroxide. MWNTs were prepared by a classical method of chemical vapor deposition.[1] *p*-Toluenesulfonic acid monohydrate (TsOH), *N*,*N*′-dicyclohexylcarbodiimide (DCC), 4-(dimethylamino)pyridine (DMAP), 4-iodophenol, PA, copper(I) iodide, triphenylphosphine, dichlorobis(triphenylphosphine)palladium-(II), 1-pyrenemethanol (**4**), 6-bromohexanoic acid, potassium hydroxide, and potassium iodide were purchased from Aldrich and used as received without further purifications. (Trimethylsilyl)-acetylene and 11-bromoundecanoic acid were both purchased from Acros. Organorhodium complexes $[Rh(nbd)Cl]_2$ (nbd = 2,5-norbornadiene) and $[Rh(cod)Cl]_2$ (cod = 1,8-cyclooctadiene) were prepared in our laboratories by literature methods.[32] 4-Ethynylbenzonic acid (**3**) was synthesized according to our previously published procedures.[33]

Instrumentation. ^{1}H and ^{13}C NMR spectra were measured on a Bruker ARX 500 NMR spectrometer using chloroform-*d* as solvent and tetramethylsilane (TMS; δ = 0 ppm) as internal standard. IR spectra were recorded on a Bruker VECTOR 22 spectrometer. UV−vis absorption spectra were measured on a Varian CARY 100 Bio UV−vis spectrophotometer. Thermal stability of the polymers was evaluated on a Perkin-Elmer Pyris thermogravimetric analyzer TGA 6. Photoluminescence spectra were recorded on Perkin-Elmer spectrofluorometer LS 55. Molecular weights (M_w and M_n) and polydispersity indexes (M_w/M_n) of the polymers were estimated in THF by a Waters gel permeation chromatography (GPC) system. A set of monodisperse polystyrene standards covering molecular weight range of 10^3-10^7 was used for molecular weight calibration.

Scanning electron microscope (SEM) images of the polymer-wrapped MWNTs were taken on a JEOL 6300L field emission SEM operating at an accelerating voltage of 5 kV, while their transmission electron microscope (TEM) images were recorded with a JEOL/JEM-200 CX TEM at an accelerating voltage of 160 kV. The TEM instrument was equipped with an EX500W CCD camera (GATAN), whose powerful imaging capability enables even biological material samples to be imaged in high resolution and contrast without staining treatment. When the image of a polymer/MWNT hybrid was observed, the beam was focused, and the optical grating of the object lens was turned down in an effort to enhance contrast. After adjusting the brightness of the image on the computer screen, a photograph was taken at the moment when a desirable image with an "ideal" contrast was captured.

Monomer and Polymer Syntheses. Monomers **1** and **2**(*m*) (*m* = 5, 10), homopolymers P**1** and P**2**(*m*), and copolymer P(**1**-*co*-PA) were prepared according to the synthetic routes shown in Schemes 1 and 2. The detailed experimental procedures and spectroscopic analysis data for the monomers and polymers are given in the Supporting Information.

Polymer/Nanotube Hybridization. Taking the preparation of P**2**(*5*)/MWNT hybrid as an example: into a tube with a stir bar were added 15 mg of P**2**(*5*), 15 mg of MWNTs, and 8 mL of THF. After stirring for half an hour, the mixture was filtered through a cotton filter to remove insoluble MWNTs. The filter was heated in an oven at 120 °C to a constant weight. The concentration of MWNTs in THF (*c*; mg/mL) was calculated by eq 1:

$$c = \frac{W_{MWNT} - (W_F - W_{F,0})}{V_S} \quad (1)$$

where W_{MWNT} (mg) is the original weight of the MWNTs, W_F and $W_{F,0}$ (mg) are the weights of the cotton filter after and before filtration, respectively, and V_s (L) is the volume of the solvent used. $(W_F - W_{F,0})$ is thus the weight of the insoluble MWNTs that were retained by the filter, and $W_{MWNT} - (W_F - W_{F,0})$ is the weight of the soluble MWNTs that passed through the filter. To learn the effect of the pyrene-containing PPA on the solubilization of MWNTs, the content of MWNTs in the MWNTs/polymer hybrid (c', %) was calculated by eq 2:

$$c' = \frac{W_{MWNT} - (W_F - W_{F,0})}{W_P + W_{MWNT} - (W_F - W_{F,0})} \times 100 \quad (2)$$

where W_P is the weight of the polymer added into the solution.

Table 1. Homopolymerization of Monomer 1 and Its Copolymerization with Phenylacetylene[a]

no.	catalyst[b]	solvent[c]	yield (%)	M_w[d]	M_w/M_n[d]
		homopolymerization			
1	$[Rh(cod)Cl]_2$	DCM/Et_3N	77.2[e]		
2	$[Rh(nbd)Cl]_2$	DCM/Et_3N	80.6[f]	11 700[g]	1.8[g]
3	$[Rh(cod)Cl]_2$	$CHCl_3$[h]	60.3	13 500	2.2
		copolymerization[i]			
4	$[Rh(cod)Cl]_2$	DCM/Et_3N	81.3	46 100	2.6
5	$[Rh(cod)Cl]_2$[j]	DCM/Et_3N	96.2	169 000	4.3
6	$[Rh(nbd)Cl]_2$	DCM/Et_3N	87.4	86 500	3.9

[a] Carried out at room temperature in an atmosphere of dry nitrogen for 24 h; $[M]_0 = 0.2$ M, [cat.] = 10 mM. [b] Abbreviations: nbd = 2.5-norborndiene and cod = 1,5-cyclooctadiene. [c] In the case of the DCM/Et_3N mixture, one drop of Et_3N was used. [d] Determined by GPC in THF on the basis of a polystyrene calibration. [e] Insoluble in DCM, chloroform, and toluene but partially soluble in THF. [f] Including insoluble and soluble products. [g] For the soluble fraction. [h] $[M]_0 = 20$ mM. [i] Molar feeding ratio of monomer **1** to PA was 3:5.5. Molar ratio of the repeat unit of **1** to that of PA in the copolymer P(**1**-*co*-PA) was determined by NMR analysis to be ~1:2. [j] [cat.] = 2 mM.

Surface Photovoltage Measurement. Surface photovoltage spectroscopy (SPS) measurement was carried out on a solid junction photovoltaic cell using a light source monochromator lock-in detection technique. The cell was in a three-layer configuration with two transparent indium−tin oxide (ITO) as electrodes, and a thin film of the hybrid was sandwiched between the two electrodes (cf. Figure 11B, inset). Monochromatic light was obtained by passing the light emitted from a 500 W xenon lamp through a double-prism monochromator (Higler & Watts D300), and a lock-in amplifier (Stanford SR 830) synchronized with a light chopper (Stanford SR 540) was employed to amplify the photovoltaic signals. Field-induced SPS (FISPS) is a technique that combines the field-effect principle with SPS. The FISPS measurement was conducted by applying an external voltage to the two sides of the cell, which was used to alter the moving direction and diffusion length of the photogenerated charge carriers.

Results and Discussion

Polymer Syntheses. PA derivatives **1** and **2**(*m*) containing pyrenyl groups were prepared by multistep reactions shown in Schemes 1 and 2. Each step of the reactions proceeded smoothly, and the desired monomers were obtained in high yields (~77−96%). To transform the monomers to polymers, we tried to use organorhodium complexes $[Rh(diene)Cl]_2$, which are known to work as effective catalysts for the polymerizations of PA derivatives of similar molecular structures, such as $HC{\equiv}CC_6H_4$-*p*-COOR (R = alkyl, aryl).[26]

We first attempted to use $[Rh(cod)Cl]_2$ to polymerize **1** in a DCM/Et_3N mixture. What disappointed us was that insoluble solid precipitated out during the polymerization reaction. As shown in Table 1, the product P**1** was insoluble in common organic solvents such as DCM and toluene and only partially soluble in THF. We then tried to use $[Rh(nbd)Cl]_2$ as catalyst, but the polymerization result was still unsatisfactory. By changing the polymerization time, we found that the solubility of the polymer was dependent on its molecular weight. When the molecular weight reached a critical value, the polymer became insoluble. On the other hand, when the molecular weight of the product was very low, the oligomer could not precipitate out from the poor solvent used for product purification. Only those with moderate molecular weights were soluble in certain solvents. To control the molecular weight of the product, we polymerized **1** without using Et_3N because it is known that the use of Et_3N usually leads to an increase in the molecular weights of PPAs.[34] Meanwhile, we decreased the concentration of **1** from 0.2 M to 20 mM by using a large amount of solvent. This "engineering control" helped: we obtained soluble P**1** when a dilute solution of **1** in chloroform alone was used as solvent (Table 1, no. 3).

Table 2. Polymerization of Monomer 2(*m*)[a]

no.	catalyst	solvent	yield (%)	M_w[b]	M_w/M_n[b]
		monomer **2**(*5*)			
1	$[Rh(cod)Cl]_2$	DCM/Et_3N	75.3	29 500	1.3
2	$[Rh(cod)Cl]_2$	THF/Et_3N	39.8	27 200	1.3
3	$[Rh(nbd)Cl]_2$	DCM/Et_3N	78.6	46 300	2.6
4	$[Rh(nbd)Cl]_2$[c]	DCM/Et_3N	95.5	136 500	4.8
		monomer**2**(*10*)			
5	$[Rh(cod)Cl]_2$	THF/Et_3N	21.6	46 900	1.5
6	$[Rh(cod)Cl]_2$	DCM/Et_3N	25.3	77 500	1.8
7	$[Rh(nbd)Cl]_2$	THF/Et_3N	18.0	99 700	2.0
8	$[Rh(nbd)Cl]_2$	DCM/Et_3N	11.4	8600	2.3
9	$[Rh(nbd)Cl]_2$[c]	DCM/Et_3N	95.2	163 800	3.5

[a] Carried out at room temperature under nitrogen for 24 h; $[M]_0 = 0.2$ M, [cat.] = 10 mM. [b] Determined by GPC in THF on the basis of a polystyrene calibration. [c] [cat.] = 2 mM.

Copolymerization is one of the most widely used strategies for improving polymer solubility because it offers a versatile means for adjusting the segmental distribution in a polymer chain. If monomer **1** is copolymerized with another monomer M**X** in a random fashion, the resultant polymer will be composed of P**1** segments that are statistically separated by P**X** segments. If the P**X** segments are soluble in a solvent that can dissolve P**1** oligomer, the copolymer should become soluble. To make sure that the backbone is a polyene, we used PA as M**X**. As can be seen from Table 1, remarkable polymerization results are obtained. The molecular weight of the copolymer P(**1**-*co*-PA) can be as high as 169 000, while the yield reaches almost quantity (96.2%; Table 1, no. 5). Most importantly, all the copolymers are highly soluble in common organic solvents such as THF, DCM, and chloroform.

The low solubility of P**1** is partially ascribable to the high rigidity of the polymer chain reinforced by the bulky pyrene pendants. Insertion of suitable flexible spacers between the pyrene pendants and the PPA skeleton may help mitigate the problem. We thus designed and synthesized monomers with long spacer lengths, viz. **2**(*5*) and **2**(*10*). The monomers can be polymerized by the organorhodium complexes in the DCM/Et_3N mixture. As can be seen from Table 2, P**2**(*5*) and P**2**(*10*) with high molecular weights are obtained in high yields. As expected, the polymers are very soluble in common organic solvents.

DCM appears to be a better solvent than THF in the polymerization of **2**(*5*), as the reactions carried out in DCM/Et_3N produces polymers with higher molecular weights in higher yields than in THF/Et_3N (cf. Table 2, nos. 1−4). The results of the polymerizations catalyzed by $[Rh(nbd)Cl]_2$ and $[Rh(cod)Cl]_2$ are comparable, when the solvent, temperature, and time are identical. The impact of catalyst concentration is, however, dramatic. The isolation yield and molecular weight of P**2**(*5*) are increased from 78.6% and 46 300 to 95.5% and 136 500, respectively, when the concentration of $[Rh(nbd)Cl]_2$ is decreased from 10 to 2 mM. This effect is more pronounced for P**2**(*10*): the isolation yield and molecular weight of P**2**(*10*) are increased from 11.4% and 8600 to 95.2% and 163 800, respectively, when the catalyst concentration is decreased by the same extent (cf. Table 2, nos. 8 and 9).

Structural Characterization. The polymeric products were characterized by spectroscopic methods. All the polymers gave satisfactory analysis data corresponding to their expected molecular structures (see Supporting Information for details). An example of the IR spectrum of P**2**(*5*) is shown in Figure 1;

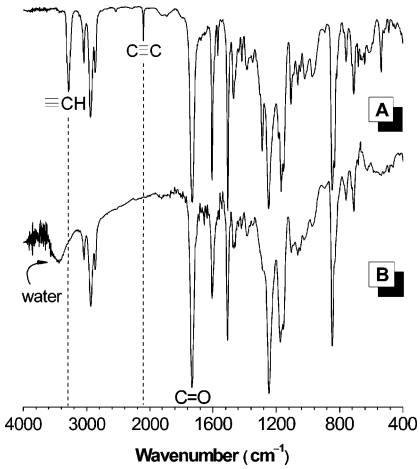

Figure 1. FT-IR spectra of (A) monomer **2**(*5*) and (B) its polymer P**2**(*5*).

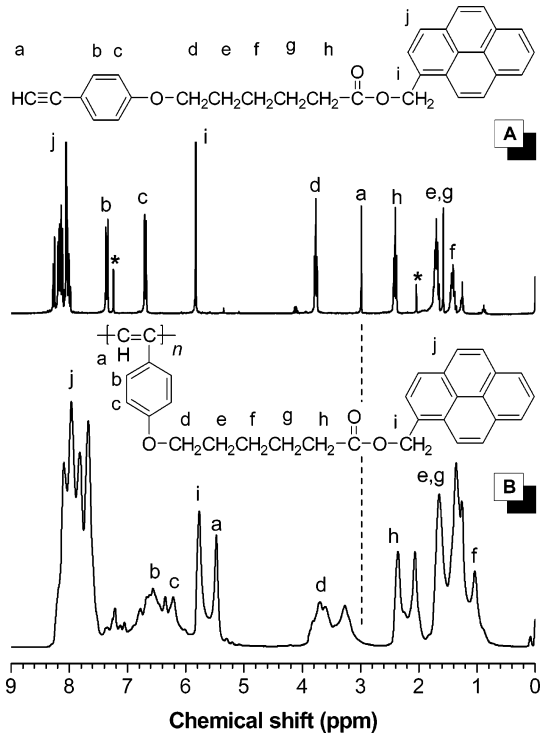

Figure 2. ^{1}H NMR spectra of (A) monomer **2**(*5*) and (B) its polymer P**2**(*5*) in chloroform-*d*. The solvent and water peaks are marked with asterisks.

the spectrum of its monomer **2**(*5*) is also given in the same figure for comparison. The monomer exhibits absorption band at 3286 and 2105 cm^{-1}, which are respectively ascribed to ≡CH and C≡C stretching vibrations. These bands completely disappear in the spectrum of P**2**(*5*), indicating that the triple bond of **2**(*5*) has been fully consumed by the polymerization reaction.

NMR spectroscopy provides valuable information about the polymer structures. As can be seen from the ^{1}H NMR spectrum of polymer P**2**(*5*), there is no resonance peak at $\delta \sim 3.0$, which is associated with the acetylene proton (Figure 2B). A new peak due to the resonance of olefinic protons appears at $\delta \sim 5.5$, which is absent in the spectrum of its monomer. The polymerization reaction transforms the acetylenic triple bond of **2**(*5*) to olefinic double bond, which upfield-shifts the resonance of the phenyl protons, which now occurs at δ 6.6 and 6.3 (Figure 2B, peaks b and c). The resonance peaks of the pyrenyl protons

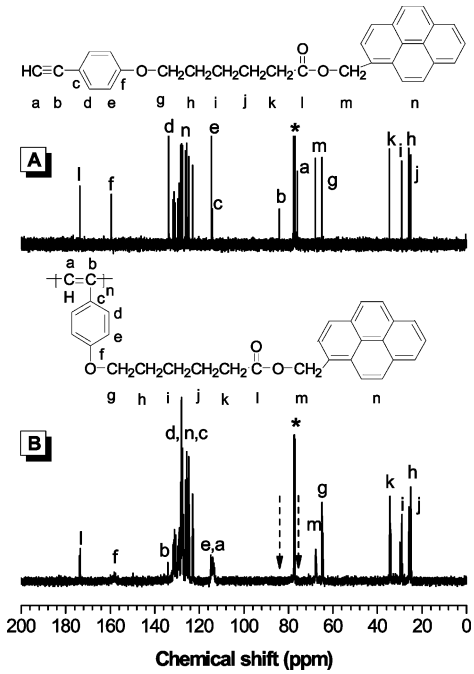

Figure 3. ^{13}C NMR spectra of (A) monomer **2**(*5*) and (B) its polymer P**2**(*5*). The solvent peaks are marked with asterisks.

also upfield shift by ~0.4 ppm upon polymerization, which should be due to the enhanced electronic interaction between the pyrenyl groups in the polymer. Like the IR spectra, the NMR spectra duly confirm that the triple bond of the monomer has been consumed by the polymerization reaction.

Figure 3 shows the ^{13}C NMR spectra of P**2**(*5*) and its monomer **2**(*5*). Whereas the acetylenic carbon atoms of **2**(*5*) resonate at δ 76.0 and 84.0, these peaks are completely absent in the spectrum of P**2**(*5*). Instead, two new peaks are observed at δ 134.2 and 113.5, which are assignable to the resonance of the polyene carbons of the polymer. This once again proves that the polymerization is realized through the transformation of the triple bonds of the monomer to the double bonds of the polymer. Since the phenyl rings are now conjugated with the polyene backbone after polymerization, the resonance of the phenyl carbons directly attached to the double bond are downfield shifted from δ 114.6 to ~126.0, as observed in our previous work.[31d,35]

Polymer/MWNT Hybridization. It is known that CNTs can be made soluble by their complexations with pyrene derivatives.[3,28] Because PPA can also solubilize CNTs,[21] it was expected that the PPAs carrying pyrene pedants would exhibit higher solvating power than their parents of pyrene derivatives. Polymer P**1**, however, shows rather small effect in solubilizing MWNTs (Figure 4). This is probably due to its rigid structure, which hampers its wrapping around the MWNT shells. The solubility of MWNTs is greatly boosted when they are wrapped by the less rigid chains of P(**1**-*co*-PA), P**2**(*5*), and P**2**(*10*). For example, 4.6 mg of MWNTs is dissolved in 8 mL of THF when the CNTs are admixed with 15 mg of P**2**(*5*), giving a solubility as high as 575 mg/L. P(**1**-*co*-PA) gives an even better result: the solubility of the MWNTs wrapped by the copolymer in THF is 637.5 mg/L. This value is respectively >3- and >11-fold higher than the solubilities of the CNTs complexed with small pyrene rings[3,28] and wrapped by pyrene-containing copolystyrene chains,[23g] revealing that there is indeed a pronounced "additive effect" of the PPA skeleton and the pyrene pendant in the hybrid.

The pristine MWNTs are insoluble in THF. They precipitate out from the polar solvent even after the forced mixing aided

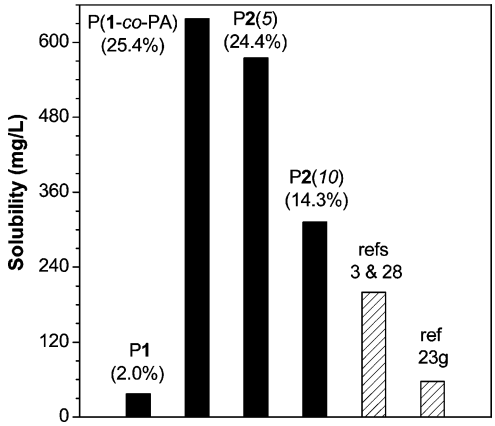

Figure 4. Solubility in THF of MWNTs wrapped in the pyrene-containing PPA chains. The contents of MWNTs in the nanohybrids given in parentheses (in %) were calculated from eq 2. The data for the CNTs wrapped by small pyrene rings[3,28] and pyrene-containing styrene copolymer chains[23g] are shown for comparison.

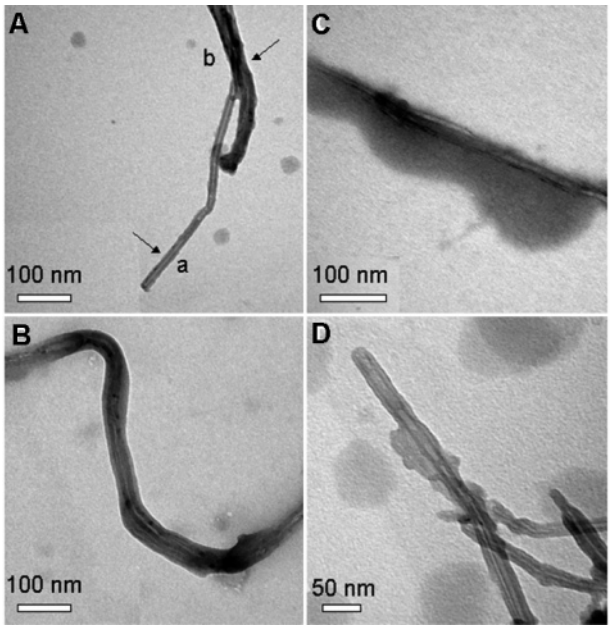

Figure 5. TEM images of MWNTs wrapped by different (co)-polymers: (A) P**1**, (B) P(**1**-*co*-PA), (C) P**2**(*5*), and (D) P**2**(*10*).

by ultrasonic irradiation. Polymer P**2**(*5*) is soluble in THF, giving a homogeneous, clear solution with a light brown color. When MWNTs are wrapped by the P**2**(*5*) chains, the CNTs become soluble in THF. The mixture is dark colored due to the existence of the MWNTs in the solution. The solution is stable for months without MWNT particles precipitating out, suggestive of intimate wrapping of the polymer chains around the CNT shells.

Morphological images of the MWNTs functionalized by different pyrene-containing PPAs are shown in Figure 5. The MWNTs are not well wrapped by the P**1** chains: some MWNTs are wrapped in a thin layer of the polymer chains (Figure 5A, spot b), while others are "naked" without any polymer chains attached (spot a). This explains why the solubility of the P**1**/MWNT hybrid in THF is low (cf. Figure 4). However, a thick layer with a contrast lower than MWNTs can be unambiguously observed in Figure 5B, whose thickness is in the range of ~10−30 nm, as deduced from the scale bar. We ascribe this layer of coating to the pyrene-containing copolymer because the carbon content of the copolymer layer is lower than that of MWNTs. The images in panels C and D of Figure 5 also show clear

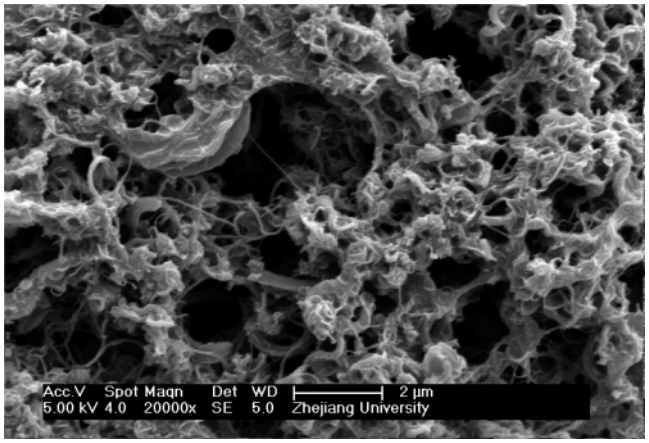

Figure 6. SEM image of the MWNTs dispersed in a P**2**(*5*) matrix. Scale bar: 2 μm.

coating layers on the MWNTs. These observations indicate that the (co)polymer chains have thickly wrapped the MWNTs. Evidently, the polymer wrapping has made the MWNTs soluble in the organic solvents.

To further examine the wrapping of the polymer chains around the MWNTs, we cast thin films of the hybrids on glass substrates from P**2**(*5*)/MWNTs solutions. The morphology of the films was checked by SEM. Porous films were deliberately prepared by fast evaporation of the volatile solvent (THF) because the coarse surfaces would allow us to view the morphological details of the films. As can be seen from the example given in Figure 6, the hybrid film is featured by interpenetrating networks with no MWNT bundles. The MWNTs are dispersed uniformly in the P**2**(*5*) matrix because they are well wrapped by the P**2**(*5*) chains. The SEM measurement further confirms that the excellent solubility of the P**2**(*5*)/MWNT hybrid in THF is due to the intimate wrapping of polymer chains around the MWNT shells.

Thermal Stability. It is known that PPA loses 5% of its weight at 225 °C (T_5).[36] The T_5 value for P**1** is 350 °C (Figure 7), which is 125 °C higher than that of PPA. Clearly, the "jacket effect" of the bulky, stable pyrene pendants surrounding the polyene backbone has helped enhance the thermal stability of the polymer.[31] The T_5 value for P(**1**-*co*-PA) is 298 °C, falling in between those of P**1** and PPA. Polymers P**2**(*5*) and P**2**(*10*) exhibit the same T_5 values (317 °C). On one hand, this indicates that the length of the methylene units in the P**2**(*m*) series exerts little effect on their T_5 values. On the other hand, when compared with P**1**, the insertion of the flexible methylene spacers between the polyene backbone and the pyrene pendants does lead to a decrease in the thermal stability of the polymer, although the effect is not to a great extent.

One of the remarkable properties of CNTs is their outstanding thermal stability. As can be seen from Figure 7, the T_5 value of the MWNTs we used in this study is as high as 782 °C. The hybridization of MWNTs with polymers should help enhance the stability of the latter. Indeed, after hybridization with the MWNTs, the thermal stability of P**2**(*5*) is enhanced. The T_5 value of P**2**(*5*)/MWNTs is 338 °C, which is >20 °C higher than that of its P**2**(*5*) parent. The experimental results thus reveal a mutual beneficial effect of the hybridization, that is, the hybridization of properly structured pyrene-containing PPA with MWNTs can improve the solubility of MWNTs as well as enhance the stability of the polymer.

Absorption and Emission. All the polymers show absorption spectra with strong peaks in the UV region and weak tails at wavelengths longer than 350 nm (Figure 8A). The absorption

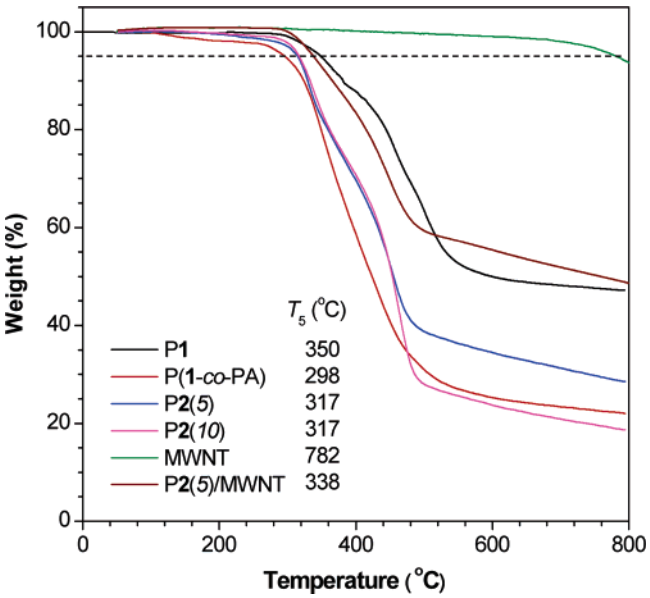

Figure 7. TGA thermograms of P**1** (sample taken from Table 1, no. 3), P(**1**-*co*-PA) (Table 1, no. 5), P**2**(*5*) (Table 2, no. 4), P**2**(*10*) (Table 2, no. 9), MWNTs, and P**2**(*5*)/MWNTs measured under nitrogen at a heating rate of 10 °C/min. T_5 denotes the temperature at which the sample loses 5% of its original weight.

peaks and tails of the polymers can be readily assigned by comparing with the absorption spectra of their monomers. An example of the monomer spectrum is given in panel B of Figure 8. The strong peaks of polymer P**2**(*5*) in the UV region are due to the absorption of its pyrene pendants because its monomer **2**(*5*) shows similar spectra in the same wavelength region. From the magnified spectra shown in the inset of Figure 8B, it can be seen that monomer **2**(*5*) does not absorb in the visible region, so the weak tail of polymer P**2**(*5*) in the long wavelength region is evidently associated with the absorption of its polyene backbone.[26] Hybrid P**2**(*5*)/MWNT absorbs more strongly than P**2**(*5*) in the visible region. This indicates that the hybrid is better conjugated than its parent polymer.[21]

Pyrene is an emissive dye, whose dilute solution gives photoluminescence spectrum featured by sharp peaks of "monomer" emission in the UV region, with a broad peak of excimer emission emerging in the visible region when its solution concentration is increased.[37] The polymers exhibit emission peaks in the UV and visible regions (Figure 9A), suggesting that the isolated "monomer" and aggregated excimer of the pyrene pendants are both involved in the light emission processes of the polymers. PPA is known to emit at ~490 nm, but the luminescence is rather weak,[38] so the peak at ~488 nm should be mainly due to the excimer emission of the pyrene pendants of the polymers rather than their PPA skeletons.

In the photoluminescence spectrum of P**1**, the emission at 488 nm dominates. This indicates that the pyrene pendants located in the immediate neighborhood of the PPA skeleton have experienced strong intrachain interaction, which has facilitated the excimer formation. This also offers a circumstantial evidence for the insolubility of the P**1** samples with high molecular weights. For copolymer P(**1**-*co*-PA), the intensity of its emission peak at 488 nm is weaker than that at 401 nm. This is easy to understand because the repeat units of **1** in the copolymer are randomly separated by those of PA, which reduces the probability for the pyrene pendants in the P**1** segments to form excimeric species. Polymers P**2**(*m*) show intermediate behaviors between those of homopolymer P**1** and copolymer P(**1**-*co*-PA). The irregular conformation of the long, flexible alkyl spacer in P**2**(*m*) may have put some of their pyrene pendants in such geographic positions where the excimers are less likely to form than in P**1**.

The emission spectra of monomer **2**(*5*) and its polymer P**2**(*5*) are compared in penal B of Figure 9. At a low concentration of 1.1×10^{-5} M, the monomer solution exhibits strong emission peaks in the UV region and a weak tail in the visible spectral region, indicating that few, if any, excimers have formed and involved in the photoluminescence process of the monomer in the dilute solution. At the same concentration, however, its polymer P**2**(*5*) exhibits a strong excimer emission peak at ~490 nm. This proves that the excimer formation in the polymer solution is mainly an intrachain event. As can be seen from the photographs shown in Figure 9B, while the solution of monomer **2**(*5*) emits a blue-violet light, the solution of its polymer P**2**(*5*) emits a blue-green light.

It is well-known that CNTs quench light emissions of conjugated polymers.[3,21,23g,28] For example, the photoluminescence of PPA was efficiently quenched by the MWNTs, although the MWNT content of the hybrid was only 6%.[21] However, in our recent study on the copolymers of CNT-containing disubstituted acetylenes, the photoluminescence of poly(1-phenyl-1-alkyne)s was found to be virtually unaffected (or not quenched) by the CNTs.[20j] Here we observed an even intriguing phenomenon: the light emission of P**2**(*5*) was enhanced by MWNTs. As can be seen from Figure 10A, the photoluminescence intensity of P**2**(*5*)/MWNT is >2-fold higher than that of its parent polymer. To make sure that this unusual result is not an experimental error, we carefully measured the fluorescence spectra of the solutions of the hybrid and polymer at various concentrations. The results always came back the same—the MWNTs enhanced, instead of quenching, the polymer's light emission, although the extent of the enhancement varied with the solution concentration (Figure 10B).

We further checked whether this was a general phenomenon for all the hybrids we prepared in this study. Using 9,10-diphenylanthracene as a standard,[26] we measured the fluorescence quantum yields (Φ_F) of P**2**(*5*)/MWNTs (Φ_F = 1.86%) and P**2**(*10*)/MWNTs (Φ_F = 1.41%), both of which were found to be higher than those of their parent polymers P**2**(*5*) (Φ_F = 1.20%) and P**2**(*10*) (Φ_F = 1.09%). The Φ_F value of P(**1**-*co*-PA)/MWNTs (0.35%) was, however, somewhat lower than that of its parent copolymer P(**1**-*co*-PA) (Φ_F = 0.45%). This verifies our early observation that MWNTs quenched the photoluminescence of PPA.[21] This quenching effect is so efficient that it even dictates the photoluminescence process in the copolymer hybrid system containing the PPA segments.

Surface Photovoltage. The excellent solubility of P**2**(*5*) and its hybrid with MWNTs in the common organic solvents allowed us to cast films from their solutions. Noticing that nanohybrids of conjugated polymers with semiconductive nanoparticles are attracting much interest for their promising applications in the field of plastic photovoltaic cells, we carried out SPS and FISPS measurements[39,40] to investigate photoinduced charge-transfer processes in the thin films of polymer P**2**(*5*) and its hybrid P**2**(*5*)/MWNTs. Figure 11A shows the FISPS spectra of a film of P**2**(*5*) under different positive biases. The spectra are comprised of broad peaks in the UV region from 320 to 360 nm, roughly resembling the absorption features of the pyrene pendants of the polymer. The similarity between the UV and FISPS spectra of the polymer suggests that the SPS signals depend on the $\pi-\pi^*$ transitions of its photoactive component. A noticeable feature of the spectra is that the intensity of the surface

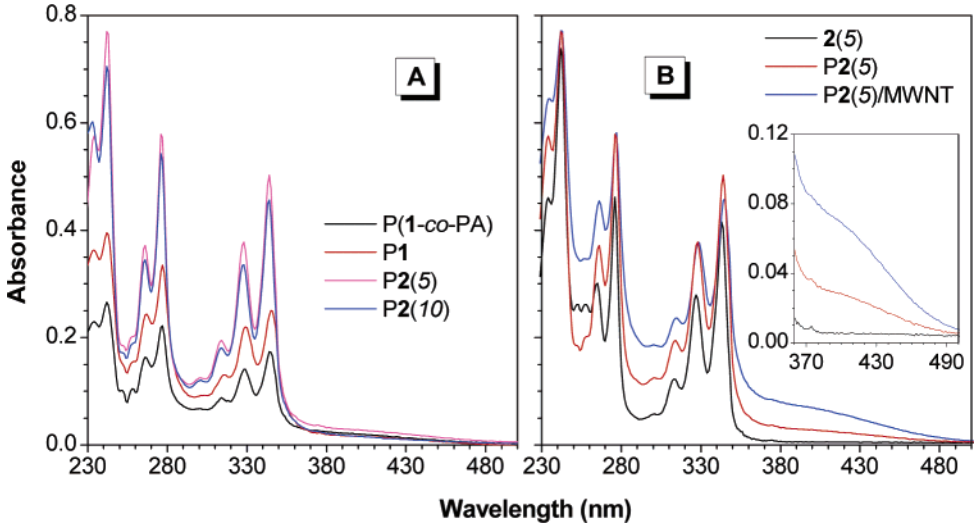

Figure 8. Absorption spectra of (A) P**1**, P(**1**-*co*-PA) and P**2**(*m*) and (B) **2**(*5*), P**2**(*5*) and P**2**(*5*)/MWNTs in THF (concentration: 11 μM). Inset in panel B is the magnified spectra in the long wavelength region.

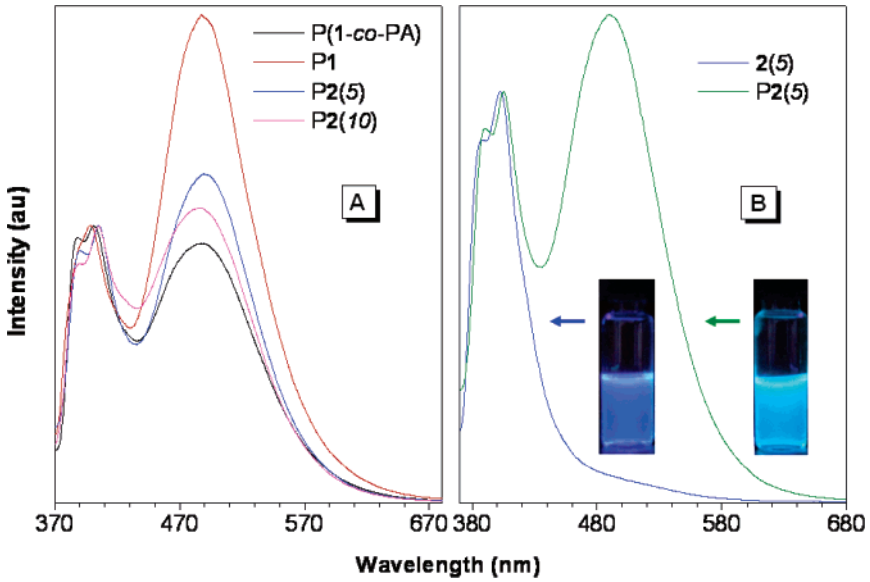

Figure 9. Photoluminescence spectra of THF solutions (11 μM) of (A) P**1**, P(**1**-*co*-PA) and P**2**(*m*) and (B) monomer **2**(*5*) and its polymer P**2**(*5*) excited at 343 nm. Examples of the photographs of the dilute THF solutions of **2**(*5*) and P**2**(*5*) taken under UV illumination are given in panel B.

photovoltage is directly proportional to the applied positive biases.

In the framework of band theory, an SPS signal is generated from the separation of the photogenerated electron−hole pairs under a built-in field, when a semiconductor is illuminated. In other words, upon photoirradiation, a change in the surface potential (δV_s) or the number of net surface charges is produced. Here, δV_s is defined as the difference between the surface potential heights before and after illumination, i.e., $\delta V_s = V_s' - V_s^0$. The magnitude of δV_s depends on the number of the net charges (or photogenerated carriers) accumulated on a semiconductor surface. For a p-type semiconductor, the surface energy bands usually bend downward, with the photogenerated electrons moving toward its surface while the holes diffusing into its bulk.[41,42] This effect leads to a positive surface photovoltaic response, i.e., $\delta V_s > 0$ (cf. Figure 12a). When a positive electric field is vertically applied to the surface of a p-type semiconductor (which is technically equivalent to applying a positive bias to the illuminated ITO electrode), the surface band bending is increased downward, and thereby the separation efficiency of the photogenerated carriers is increased because the direction of the applied field coincides with that of the built-in field. As a result, the intensity of the surface photovoltaic response is increased (Figure 12b). Our experimental results are in precise agreement with the theoretic prediction.

In contrast, when a negative bias was applied to the surface photovoltaic cell, very small changes in the intensity of surface photovoltaic response were recorded. As can be seen from Figure 11B, the surface photovoltaic responses under zero and negative biases are similar. This phenomenon can be explained as follows. Because the direction of the applied electric field is opposite to that of the built-in field, the surface band bending is decreased (cf. Figure 12c), and the separation efficiency of the photogenerated electron−hole pairs is hence decreased. As a result, the number of the net charges accumulated on the surface is small, and the applied field thus exerts a smaller effect on the surface photovoltaic responses as compared to the case of the positive bias. Our photovoltaic cell is a unipolar device because only P**2**(*5*) or a p-semiconductor is sandwiched between two electrodes. The externally reversed field thus results in an unsymmetrical response to the same illumination.

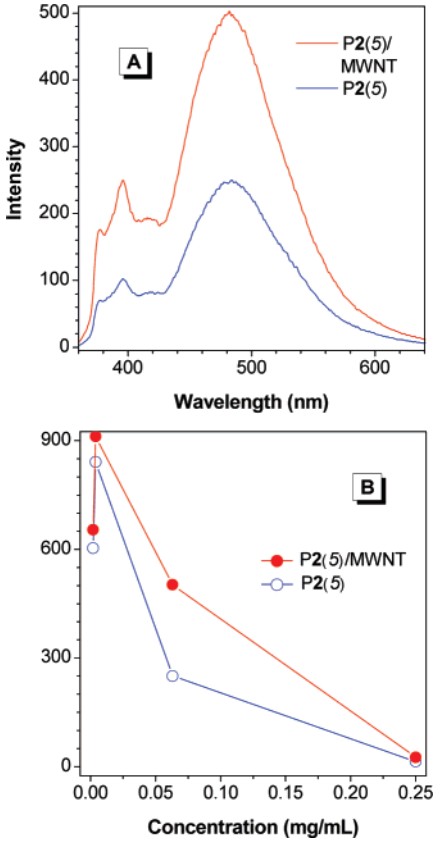

Figure 10. (A) Photoluminescence spectra of THF solutions (0.063 mg/mL) of P**2**(*5*)/MWNT and P**2**(*5*) excited at 344 nm and (B) dependence of the emission intensity at 488 nm on the solution concentration.

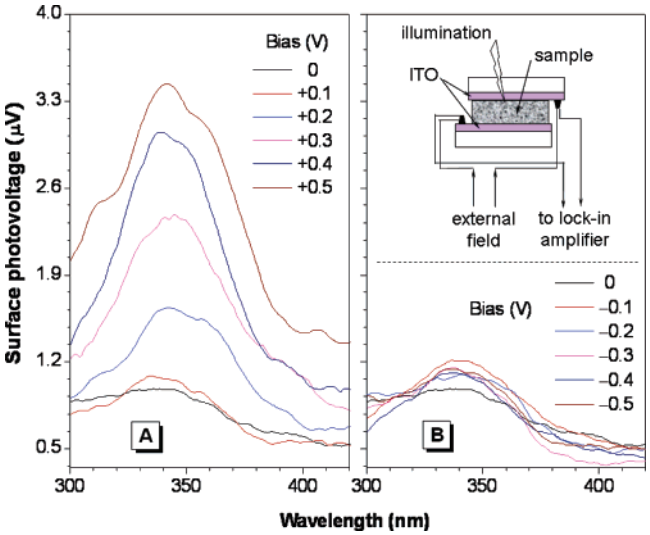

Figure 11. Surface photovoltages of thin films of polymer P**2**(*5*) sandwiched between ITO electrodes under (A) positive and (B) negative biases. The signs of positive (+) and negative (−) are defined as the application of positive and negative biases, respectively, to the illuminated ITO electrodes. Shown in the inset in the upper part of panel B is a diagrammatic illustration for the surface photovoltage measurement.

However, when the thin film of the P**2**(*5*)/MWNT hybrid was used in the surface photovoltaic cell, the situation dramatically changed. From the surface photovoltage action spectra shown in panels A and B of Figure 13, two new characteristics are readily noticeable. First, the surface photovoltage signals show symmetrical responses to the external fields: both positive and negative biases result in an increase in the surface photovoltage. This reveals that the device is now bipolar. The active layer is now comprised of two components, P**2**(*5*) and MWNTs: the former and the latter can be respectively regarded as p- and n-type semiconductors. Thanks to the high loading of MWNTs in the hybrid and its excellent solubility in the solvent, the p-type P**2**(*5*) and n-type MWNTs have formed an interpenetrating network in the film, as disclosed by the SEM analysis (cf. Figure 6). This enables the two components to disperse uniformly throughout the hybrid film and to independently respond to the external fields, both positive and negative.

The second characteristic is that the magnitude of the surface photovoltage in the hybrid is smaller than that of the pristine polymer. Under zero bias, for example, the maximum surface photovoltage for the P**2**(*5*) film is 0.98 μV, while for the P**2**(*5*)/MWNT hybrid, this value is dropped to 0.27 μV. Even with the aid of the external fields, the magnitudes of the recorded surface photovoltage are lower than 0.9 μV. These results imply that the photogenerated carriers have a small contribution to the surface photovoltage.

According to the principles of the SPS and FISPS processes, the photogenerated species can cause only a small change in the number of net surface charges.[39,40] Comparing these two sets of experiments, the only difference lies in the MWNT component. Because of its n-type nature, the MWNTs play a role of electron acceptors in the hybrids.[43,44] When the photovoltaic cell is illuminated, the pyrene pendants attached to the polymer chains are photoexcited and the electron−hole pairs are formed and subsequently disassociated by the built-in field. However, in the P**2**(*5*)/MWNT hybrid, the generated electrons are transferred to the acceptors or MWNTs but not contributed to the neutralization of surface positive charges, which are of significance to the changes in the number of the net surface charges. As a result, much smaller surface photovoltage signals are recorded in the hybrid device.

Concluding Remarks

In this work, we synthesized a group of pyrene-containing PPAs using the organorhodium complexes as catalysts. When the pyrene group is linked to PA without a flexible spacer, the monomer (**1**) can be polymerized but the polymer (P**1**) with high molecular weight is insoluble in common organic solvents. The copolymerization of **1** with PA under similar conditions afforded copolymers P(**1**-*co*-PA) with high molecular weights and excellent solubility in yields up to ~96%. The monomers with long alkyl spacers [**2**(*m*)] were efficiently polymerized, and the resultant polymers [P**2**(*m*)] were completely soluble. The hybridization of these (co)polymers with MWNTs helped make the CNTs highly soluble in common organic solvents such as THF and chloroform. The maximum solubility is 637.5 mg/L in THF, which is the highest among all the solubility data reported for the CNTs functionalized by small pyrene rings[45] and wrapped by pyrene-containing polymer chains.[20,23g] This is attributable to the "additive affect" of the pyrene pendants and the PPA skeleton[21,45] in solubilizing the CNTs.

The TEM images of the hybrids clearly show that the MWNTs are wrapped in a thin polymer layer, with the extent of wrapping depending on the polymer structure. The SEM photographs further confirm the coating of polymer layers on the surfaces of the MWNTs and reveal the formation of interpenetrating networks between the polymers and the MWNTs. The UV spectra of the polymers are dominated by the absorption feature of the pyrene pendants in the wavelength region of ~320−350 nm. The hybrid absorbs more intensely in the visible

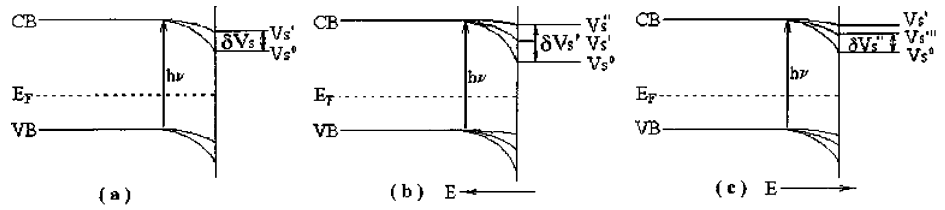

Figure 12. Schematic representations of energy band modes of a p-type semiconductor with a Schottky-type barrier under application of (a) zero, (b) positive, and (c) negative biases. Symbols: δV_s ($\delta V_s'$, $\delta V_s''$) = surface potential difference, V_s^0 = surface potential height before illumination, V_s' (V_s'', V_s''') = surface potential height after illumination, CB = conduction band, VB = valence band, and E_F = Fermi level.

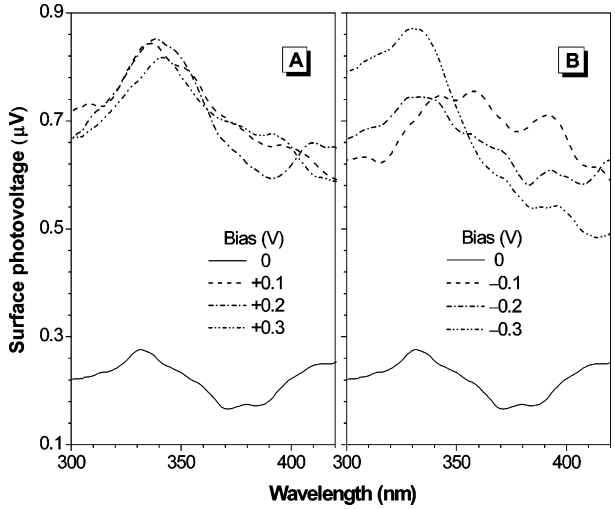

Figure 13. Surface photovoltages of thin film of hybrid P**2**(*5*)/MWNT sandwiched between two ITO electrodes under (A) positive and (B) negative biases.

region, thanks to the electronic conjugation enhanced by the favorable $\pi-\pi$ interactions between the polymer chains and the MWNT shells. The photoluminescence spectra of the polymers are characterized by the monomer and excimer emissions in the UV and visible regions. Upon photoexcitation, the P**2**(*m*)/MWNT hybrids emit brighter blue-green light in higher efficiencies than do their parent polymers P**2**(*m*).

The FISPS spectra reveal the unipolar characteristic of the P**2**(*5*)-based surface photovoltaic cell. The cell of the P**2**(*5*)/MWNT hybrid is, however, bipolar in nature because the surface photovoltage signal change symmetrically with the directions of the externally applied biases. This is the result of the hybridization of a large amount of n-type MWNTs with the p-type P**2**(*5*) and the formation of well-interpenetrated networks of the two components. The magnitude of surface photovoltage of the bipolar cell is evidently smaller than that of its unipolar counterpart. This suggests that there exists an efficient photoinduced charge transfer between the P**2**(*5*) donor and the MWNT acceptor in the bulk because the photogenerated carriers have not contributed to the variation in the surface photovoltage.

Clearly, the noncovalent functionalization of MWNTs by the pyrene-containing PPAs has enabled the preparation of the nanohybrids with combined properties of their constituent components. The excellent solubility of the hybrids with high loading of MWNTs in common solvents has facilitated the fabrication of hybrid films with interpenetrating network structure. Our approach thus offers a versatile means for hybridizing a large amount of noncovalently functionalized MWNTs with conjugated polymers. We are now exploring the possibility of using the hybrids to construct new photoelectronic devices for high-tech applications.

Acknowledgment. This work reported in this paper was partially supported by the Ministry of Science & Technology of China (Project No. 2002CB613401), the Nation Natural Science Foundation of China (Project Nos. 20634020 and 50573065), and the Research Grants Council of Hong Kong (Project Nos. 602706, HKU2/05C, 603505, and 603304). B.Z.T. thanks the support of the Cao Guangbiao Foundation of the Zhejiang University.

Supporting Information Available: Experimental procedures for the syntheses of the intermediates, monomers, and polymers and detailed characterization data for all the new monomers and polymers. This material is available free of charge via the Internet at http://pubs.acs.org.

References and Notes

(1) (a) *Carbon Nanotubes: Preparation and Properties*; Ebbesen, T. W., Ed.; CRC Press: Boca Raton, FL, 1997. (b) *Carbon Nanotubes: Basic Concepts and Physical Properties*; Reich, S., Thomsen, C., Maultzsch, J., Eds.; VCH: Weinheim, Germany, 2004.

(2) (a) Andrews, R.; Jacques, D.; Qian, D.; Rantell, T. *Acc. Chem. Res.* **2002**, *35*, 1008−1017. (b) Ouyang, M.; Huang, J.-L.; Lieber, C. M. *Acc. Chem. Res.* **2002**, *35*, 1018−1025. (c) Avouris, P. *Acc. Chem. Res.* **2002**, *35*, 1026−1034. (d) Dai, H. *Acc. Chem. Res.* **2002**, *35*, 1035−1044. (e) Sun, Y.-P.; Fu, K.; Lin, Y.; Huang, W. *Acc. Chem. Res.* **2002**, *35*, 1096−1104.

(3) Guldi, D. M.; Rahman, G. M. A.; Zerbetto, F.; Prato, M. *Acc. Chem. Res.* **2005**, *38*, 871−878.

(4) Grossiord, N.; Loos, J.; Regev, O.; Koning, C. E. *Chem. Mater.* **2006**, *18*, 1089−1099.

(5) Guldi, D. M.; Rahman, G. M. A.; Sgobba, V.; Kotov, N. A.; Bonifazi, D.; Prato, M. *J. Am. Chem. Soc.* **2006**, *128*, 2315−2323.

(6) Rahman, G. M. A.; Guldi, D. M.; Zambon, E.; Pasquato, L.; Tagmatarchis, N.; Prato, M. *Small* **2005**, *1*, 527−530.

(7) Wu, W.; Zhang, S.; Li, Y.; Li J. *Macromolecules* **2003**, *36*, 6286−6288.

(8) (a) Kong, J.; Franklin, N. R.; Zhou, C. W.; Chapline, M. G.; Peng, S.; Cho, K. J.; Dai, H. J. *Science* **2000**, *287*, 622−625. (b) Wang, J.; Musameh, M.; Lin, Y. *J. Am. Chem. Soc.* **2003**, *125*, 2408−2409. (d) Goldoni, A.; Larciprete, R.; Petaccia, L.; Lizzit, S. *J. Am. Chem. Soc.* **2003**, *125*, 11329−11333.

(9) (a) Campbell, J. K.; Sun, L.; Crooks, R. M. *J. Am. Chem. Soc.* **1999**, *121*, 3779−3780. (b) Tu, Y.; Lin, Y.; Ren, Z. F. *Nano Lett.* **2003**, *3*, 107−109. (c) Lin, Y.; Lu, F.; Tu, Y.; Ren, Z. *Nano Lett.* **2004**, *4*, 191−195. (d) Heller, I.; Kong, J.; Heering, H. A.; Williams, K. A.; Lemay, S. G.; Dekker: C. *Nano Lett.* **2005**, *5*, 137−142. (e) Heller, I.; Kong, J.; Williams, K. A.; Dekker: C.; Lemay, S. G. *J. Am. Chem. Soc.* **2006**, *128*, 7353−7359.

(10) (a) Shim, M.; Javey, A.; Shi Kam, N. W.; Dai, H. *J. Am. Chem. Soc.* **2001**, *123*, 11512−11513. (b) Nojeh, A.; Lakatos, G. W.; Peng, S.; Cho, K.; Pease, R. F. W. *Nano Lett.* **2003**, *3*, 1187−1190.

(11) Yang, X.; Guillorn, M. A.; Austin, D.; Melechko, A. V.; Cui, H.; Meyer, H. M.; III.; Merkulov, V. I.; Caughman, J. B. O.; Lowndes, D. H.; Simpson, M. L. *Nano Lett.* **2003**, *3*, 1751−1755.

(12) Martin, B. B.; Qu, L.; Lin, Y.; Harruff, B. A.; Bunker, C. E.; Gord, J. R.; Allard, L. F.; Sun Y.-P. *J. Phys. Chem. B* **2004**, *108*, 11447−11453.

(13) (a) Ago, H.; Petritsch, K.; Shaffer, M. S. P.; Windle, A. H.; Friend, R. H. *Adv. Mater.* **1999**, *11*, 1281−1285. (b) Kymakis, E.; Alexandrou, I.; Amaratunga, G. A. J. *J. Appl. Phys.* **2003**, *93*, 1764−1768.

(14) (a) Star, A.; Stoddart, J. F.; Steuerman, D. W.; Diehl, M. R.; Boukai, A.; Wong, E. W.; Yang, X.; Chung, S.-W.; Choi, H.; Heath, J. R. *Angew. Chem., Int. Ed.* **2001**, *40*, 1721−1725. (b) Star, A.; Liu, Y.;

Grant, K.; Ridvan, L.; Stoddart, J. F.; Steuerman, D. W.; Diehl, M. R.; Boukai, A.; Heath, J. R. *Macromolecules* **2003**, *36*, 553−560.
(15) Guldi, D. M.; Marcaccio, M.; Paolucci, D.; Paolucci, F.; Tagmatarchis, N.; Tasis, D.; Vazquez, E.; Prato, M. *Angew. Chem., Int. Ed.* **2003**, *42*, 4206−4209.
(16) Zhu, W.; Minami, N.; Kazaoui, S.; Kim, Y. *J. Mater. Chem.* **2003**, *13*, 2196−2201.
(17) Alvaro, M.; Atienzar, P.; Bourdelande, J. L.; Garcia, H. *Chem. Phys. Lett.* **2004**, *384*, 119−123.
(18) Li, H.; Zhou, B.; Lin, Y.; Gu, L.; Wang, W.; Fernando, K. A. S.; Kumar, S.; Allard, L. F.; Sun, Y.-P. *J. Am. Chem. Soc.* **2004**, *126*, 1014−1015.
(19) Hirsch, A. *Angew. Chem., Int. Ed.* **2002**, *41*, 1853−1859.
(20) (a) Lin, Y.; Zhou, B.; Shiral Fernando, K. A.; Liu, P.; Allard, L. F.; Sun, Y.-P. *Macromolecules* **2003**, *36*, 7199−7204. (b) Kong, H.; Gao, C.; Yan, D. *J. Am. Chem. Soc.* **2004**, *126*, 412−413. (c) Liu, Y.; Adronov, A. *Macromolecules* **2004**, *37*, 4755−4760. (d) Xu, Y.; Gao, C.; Kong, H.; Yan, D.; Jin, Y. Z.; Watts, P. C. P. *Macromolecules* **2004**, *37*, 8846−8853. (e) Qin, S.; Qin, D.; Ford, W. T.; Herrera, J. E.; Resasco, D. E. *Macromolecules* **2004**, *37*, 9963−9967. (f) Liu, Y.; Yao, Z.; Adronov, A. *Macromolecules* **2005**, *38*, 1172−1179. (g) Buffa, F.; Hu, H.; Resasco, D. E. *Macromolecules* **2005**, *38*, 8258−8263. (h) Qu, L.; Veca, L. M.; Lin, Y.; Kitaygorodskiy, A.; Chen, B.; McCall, A. M.; Connell, J. W.; Sun, Y.-P. *Macromolecules* **2005**, *38*, 10328−10331. (i) Zhang, H.; Li, H. X.; Cheng, H. M. *J. Phys. Chem. B* **2006**, *110*, 9095−9099. (j) Li, Z.; Dong, Y.; Haussler, M.; Lam, J. W. Y.; Dong, Y.; Wu, L.; Wong, K. S.; Tang, B. Z. *J. Phys. Chem. B* **2006**, *110*, 2302−2309.
(21) Tang, B. Z.; Xu, H. *Macromolecules* **1999**, *32*, 2569−2576.
(22) (a) Curran, S. A.; Ajayan, P. M.; Blau, W. J.; Carroll, D. L.; Coleman, J. N.; Dalton, A. B.; Davey, A. P.; Strevens, A. *Adv. Mater.* **1998**, *10*, 1091−1093. In this work, the authors dramatically boosted the conductivity of poly[*m*-phenylenevinylene-*co*-(2,5-dioctoxy-*p*-phenylenevinylene)] by a factor of 10^8 through its composition with CNTs, although the photoluminescence of the polymer was partially quenched by the CNTs. (b) Tasis, D.; Tagmatarchis, N.; Georgakilas, V.; Prato, M. *Chem.—Eur. J.* **2003**, *9*, 4000−4008.
(23) (a) Chen, R. J.; Zhang, Y.; Wang, D.; Dai, H. *J. Am. Chem. Soc.* **2001**, *123*, 3838−3839. (b) Chen, J.; Liu, H.; Weimer, W. A.; Halls, M. D.; Waldeck, D. H.; Walker, G. C. *J. Am. Chem. Soc.* **2002**, *124*, 9034−9035. (c) Fifield, L. S.; Dalton, L. R.; Addleman, R. S.; Galhotra, R. A.; Engelhard, M. H.; Fryxell, G. E.; Aardahl, C. L. *J. Phys. Chem. B* **2004**, *108*, 8737−8741. (d) Lou, X.; Daussin, R.; Cuenot, S.; Duwez, A.-S.; Pagnoulle, C.; Detrembleur, C.; Bailly, C.; Jerome, R. *Chem. Mater.* **2004**, *16*, 4005−4011. (e) Guldi, D. M.; Rahman, G. M. A.; Jux, N.; Balbinot, D.; Tagmatarchisc, N.; Prato, M. *Chem. Commun.* **2005**, 2038−2040. (f) Wang, T.; Hu, X.; Qu, X.; Dong, S. *J. Phys. Chem. B* **2006**, *110*, 6631−6636. (g) Bahun, G. J.; Wang, C.; Adronov, A. *J. Polym. Sci., Part A: Polym. Chem.* **2006**, *44*, 1941−1951. (h) Cheng, F.; Zhang, S.; Adronov, A.; Echegoyen, L.; Diederich, F. *Chem.—Eur. J.* **2006**, *12*, 6062−6070. (i) Cheng, F.; Adronov, A. *Chem.—Eur. J.* **2006**, *12*, 5053−5059.
(24) (a) Panhuis, M.; Maiti, A.; Dalton, A. B.; van den Noort, A.; Coleman, J. N.; McCarthy, B.; Blau, W. J. *J. Phys. Chem. B* **2003**, *107*, 478−482. (b) Bhattacharyya, S.; Kymakis, E.; Amaratunga, G. A. J. *Chem. Mater.* **2004**, *16*, 4819−4823. (c) Valentini, L.; Armentano, I.; Biagiotti, J.; Marigo, A.; Santucci, S.; Kenny, J. M. *Diam. Relat. Mater.* **2004**, *13*, 250−255. (d) Kymakis, E.; Amaratunga, G. A. J. *Synth. Met.* **2004**, *142*, 161−167. (e) Xu, Z.; Wu, Y.; Hua, B.; Ivanov, I. N.; Geohegan, D. B. *Appl. Phys. Lett.* **2005**, *87*, 263118. (f) Pradhan, B.; Batabyal, S. K.; Pal, A. J. *J. Phys. Chem. B* **2006**, *110*, 8274−8277.
(25) Zerza, G.; Rothler, B.; Sariciftci, N. S.; Gomez, R.; Segura, J. L.; Martin, N. *J. Phys. Chem. B* **2001**, *105*, 4099−4104 and references therein.
(26) For reviews, see: (a) Lam, J. W. Y.; Tang, B. Z. *Acc. Chem. Res.* **2005**, *38*, 745−754. (b) Lam, J. W. Y.; Tang, B. Z. *J. Polym. Sci., Part A: Polym. Chem.* **2003**, *41*, 2607−2629. (c) Cheuk, K. K. L.; Li, B. S.; Tang, B. Z. *Curr. Trends Polym. Sci.* **2002**, *7*, 41−55. (d) Tang, B. Z. *Polym. News* **2001**, *26*, 262−272.
(27) Lam, J. W. Y.; Peng, H.; Häussler, M.; Zheng, R.; Tang, B. Z. *Mol. Cryst. Liq. Cryst.* **2004**, *415*, 43−60.
(28) Guldi, D. M.; Rahman, G. M. A.; Jux, N.; Balbinot, D.; Hartnagel, U.; Tagmatarchis, N.; Prato, M. *J. Am. Chem. Soc.* **2005**, *127*, 9830−9838.
(29) Huang, M. H.; Dunn, B. S.; Zink, J. I. *J. Am. Chem. Soc.* **2000**, *122*, 3739−3745.
(30) Matsui, J.; Mitsuishi, M.; Miyashita, T. *Macromolecules* **1999**, *32*, 381−386.
(31) (a) Lam, J. W. Y.; Dong, Y.; Cheuk, K. K. L.; Luo, J.; Xie, Z.; Kwok, H. S.; Mo, Z.; Tang, B. Z. *Macromolecules* **2002**, *35*, 1229−1240. (b) Lam, J. W. Y.; Kong, X.; Dong, Y.; Cheuk, K. K. L.; Xu, K.; Tang, B. Z. *Macromolecules* **2000**, *33*, 5027−5040. (c) Lam, J. W. Y.; Luo, J.; Dong, Y.; Cheuk, K. K. L.; Xu, K.; Tang, B. Z. *Macromolecules* **2002**, *35*, 8288−8299. (d) Lam, J. W. Y.; Dong, Y.; Cheuk, K. K. L.; Law, C. C. W.; Lai, L. M.; Tang, B. Z. *Macromolecules* **2004**, *37*, 6695−6704. (e) Law, C. C. W.; Lam, J. W. Y.; Dong, Y.; Tong, H.; Tang, B. Z. *Macromolecules* **2005**, *38*, 660−662.
(32) *Dictionary of Organometallic Compounds*, 2nd ed.; Chapman & Hall: London, 1995.
(33) Tang, B. Z.; Kong, X.; Wan, X.; Feng, X.-D. *Macromolecules* **1997**, *30*, 5620−5628.
(34) Cheuk, K. K. L.; Lam, J. W. Y.; Lai, L. M.; Dong, Y.; Tang, B. Z. *Macromolecules* **2003**, *36*, 9752−9762.
(35) Kong, X.; Lam, J. W. Y.; Tang, B. Z. *Macromolecules* **1999**, *32*, 1722−1730.
(36) Masuda, T.; Tang, B. Z.; Higashimura, T.; Yamaoka, H. *Macromolecules* **1985**, *18*, 2369−2373.
(37) (a) Winnik, M. A.; Bystryak, S. M.; Liu, Z. *Macromolecules* **1998**, *31*, 6855−6864. (b) Berlman, I. B. *Handbook of Fluorescence Spectra of Aromatic Molecules*; Academic Press: New York, 1971.
(38) Lee, C. W.; Wong, K. S.; Lam, W. Y.; Tang, B. Z. *Chem. Phys. Lett.* **1999**, *307*, 67−74.
(39) (a) Kronik, L.; Shapira, Y. *Surf. Sci. Rep.* **1999**, *37*, 1−216. (b) Kronik, L.; Shapira, Y. *Surf. Interface Anal.* **2001**, *31*, 954−991.
(40) (a) Zhang, J.; Wang, D. J.; Shi, T. S.; Wang, B. H.; Sun, J. Z.; Li, T. J. *Thin Solid Films* **1996**, *284/285*, 596−599. (b) Zhang, J.; Wang, D. J.; Chen, Y. M.; Li, T. J.; Mao, H. F.; Tian, H. J.; Zhou, Q. F.; Xu, H. *Thin Solid Films* **1997**, *300*, 208−212.
(41) Lin, Y.; Wang, D.; Zhao, Q.; Yang, M.; Zhang, Q. *J. Phys. Chem. B* **2004**, *108*, 3202−3206.
(42) Xie, T. F.; Wang, D. J.; Zhu, L. J.; Wang, C.; Li, T. J.; Zhou, X. Q.; Wang, M. *J. Phys. Chem. B* **2000**, *104*, 8177−8181.
(43) Cao, L.; Chen, H. Z.; Wang, M.; Sun, J. Z.; Zhang, X. B.; Kong, F. Z. *J. Phys. Chem. B* **2002**, *106*, 8971−8975.
(44) Cao, J.; Sun, J. Z.; Hong, J.; Li, H. Y.; Chen, H. Z.; Wang, M. *Adv. Mater.* **2004**, *16*, 84−87.
(45) Tasis, D.; Tagmatarchis, N.; Bianco, A.; Prato, M. *Chem. Rev.* **2006**, *106*, 1105−1136.

MA061856C